Acta Biomaterialia 57 (2017) 352–362

Contents lists available at ScienceDirect

Acta Biomaterialia

journal homepage: www.elsevier.com/locate/actabiomat

Full length article

Dynamic fatigue measurement of human erythrocytes using dielectrophoresis

Yuhao Qiang, Jia Liu, E Du *

Department of Ocean and Mechanical Engineering, Florida Atlantic University, Boca Raton, FL 33431, USA

ARTICLE INFO

Article history:
Received 2 December 2016
Received in revised form 15 May 2017
Accepted 15 May 2017
Available online 17 May 2017

Keywords:
Dielectrophoresis
Microfluidics
Dynamic fatigue measurement
Erythrocytes
Biomechanics

ABSTRACT

Erythrocytes must undergo severe deformation to pass through narrow capillaries and submicronic splenic slits for several hundred thousand times in their normal lifespan. Studies of erythrocyte biomechanics have been mainly focused on cell deformability and rheology measured from a single application of stress and mostly under a static or quasi-static state using classical biomechanical techniques, such as optical tweezers and micropipette aspiration. Dynamic behavior of erythrocytes in response to cyclic stresses that contributes to the membrane failure in blood circulation is not fully understood. This paper presents a new experimental method for dynamic fatigue analysis of erythrocytes, using amplitude modulated electrokinetic force field in a microfluidic platform. We demonstrate the capability of this new technique using a low cycle fatigue analysis of normal human erythrocytes and ATP-depleted erythrocytes. Cyclic tensile stresses are generated to induce repeated uniaxial stretching and extensional recovery of single erythrocytes. Results of morphological and biomechanical parameters of individually tracked erythrocytes show strong correlations with the number of the loading cycles. Under a same strength of electric field, after 180 stress cycles, for normal erythrocytes, maximum stretch ratio decreases from 3.80 to 2.86, characteristic time of cellular extensional recovery increases from 0.16 s to 0.37 s, membrane shear viscosity increases from 1.0 (μN/m) s to 1.6 (μN/m) s. Membrane deformation in a small number of erythrocytes becomes irreversible after large deformation for about 200 cyclic loads. ATP-depleted cells show similar trends in decreased deformation and increased characteristic time with the loading cycles. These results show proof of concept of the new microfluidics technique for dynamic fatigue analysis of human erythrocytes.

Statement of significance

Red blood cells (RBCs) experience a tremendous number of deformation in blood circulation before losing their mechanical deformability and eventually being degraded in the reticuloendothelial system. Prior efforts in RBC biomechanics have mostly focused on a single-application of stress, or quasi-static loading through physical contact to deform cell membranes, thus with limited capabilities in probing cellular dynamic responses to cyclic stresses. We present a unique electrokinetic microfluidic system for the study of dynamic fatigue behavior of RBCs subjected to cyclic loads. Our work shows quantitatively how the cyclic stretching loads cause membrane mechanical degradation and irreversibly deformed cells. This new technique can be useful to identify biomechanical markers for prediction of the mechanical stability and residual lifespan of circulating RBCs.

1. Introduction

Erythrocytes, or red blood cells (RBCs) must undergo passive deformation while maintaining their mechanical stability as they pass through the systemic and pulmonary circulations. They are subjected to severe deformation during squeezing through narrow capillaries down to 3 μm diameter and endothelial slits of 0.5 μm wide [1]. During the repeated passages for several hundred thousand times in their 120-day normal lifespan, cumulative effects from mechanical stresses and a series of biological or biochemical modifications cause a discocyte-echinocyte morphological transformation as well as mechanical degradation in RBC membranes [2]. Cell rigidification along with the discocyte-echinocyte

* Corresponding author.
E-mail address: edu@fau.edu (E Du).

http://dx.doi.org/10.1016/j.actbio.2017.05.037
1742-7061/

transformation has been considered as an index of RBC membrane failure and a key biomechanical aspect of eryptosis, suicidal death of erythrocytes [3]. Such mechanical degradation in cell membranes are accelerated in various pathological conditions, such as malaria [4], sickle cell anemia [5], hypertension [6], and diabetes [7], as well as many physiological conditions, such as extracorporeal circuit for hemodialysis [8] and cardiopulmonary bypass [9].

Characterization of the mechanical properties of RBCs has been the subject of intense study for decades [10–13]. RBC deformability, the ability to change cellular shape in response to applied stress without hemolysis, is primarily regulated by three constitutive characteristics, including membrane deformability, cell surface area to volume ratio, and cytoplasmic viscosity [1]. Many experimental strategies have been developed to probe the mechanics of single RBCs, cell suspensions, or subcellular components. The most classical methods to characterize RBC membrane mechanics are micropipette aspiration [14] and optical tweezers [5,15,16]. In micropipette aspiration, part of cell membrane is aspired into a micropipette under a hydrostatic pressure difference. Mechanical properties of cell membranes can be estimated based on membrane deformation during aspiration and on the subsequent relaxation from large deformation. Membrane shear modulus of normal RBCs was estimated to be 2.4–11.3 μN/m, the characteristic time of membrane relaxation was about 0.1–0.3 s, and the corresponding membrane viscosity was about 0.3–2.8 (μN/m) s [17,18]. In optical tweezers, imposed tensile stretching on single RBCs was achieved by moving in opposite directions the two beads attached to cell membranes. Membrane shear elastic modulus of normal RBCs was estimated to be 2.5 ± 0.4 μN/m using small forces of 10–15 pN [19], 8.5 μN/m using forces no more than 200 pN [20], and 13.3 μN/m using forces up to 340 pN [15]. Other methods such as atomic force microscopy [21], ektacytometry [22], and magnetic twisting cytometry [23] and diffraction phase microscopy [24], were reviewed by other researchers [25,26]. The metabolic state of RBCs, determined by the level of adenosine 5′-triphosphate (ATP), can significantly affect cellular deformability, demonstrated experimentally [27,28] and using theoretical models [29,30]. Comparing to normal RBCs, it has been found that the shear modulus of ATP-depleted RBCs increased by 17% and shear viscosity in plastic domain decreased by 32%, determined by micropipette aspiration and flow channel techniques [31]. Comparing to normal RBCs, membrane fluctuation amplitude has been found to decrease significantly in RBCs absent of ATP [32,33] and increase in ATP-repleted cells [34]. These studies have largely advanced our understanding of the mechanical basis of RBCs in macro- and microcirculation. However, many of these systems are not well suited to probe fatigue behavior of cells, with limitations in quasi-static loading through physical contact to deform the cells or relying on membrane thermal fluctuations to probe the linear regime behavior.

Dynamic behavior in response to cyclic stresses, an important aspect of RBC biomechanics that contributes to RBC membrane failure during *in vivo* circulation and extracorporeal circulation is still largely unknown. To our knowledge, fatigue analysis of erythrocytes has not been implemented yet in other systems, such as optical tweezers and micropipette aspiration. A few recent studies have reported characterization of membrane damage in RBCs under cyclic loading using shear flow in a narrow microfluidic channel [35] and in a high-viscosity rheoscope system [36].The reported results were limited to cell morphological deformation and recovery. Both approaches rely on shear flow to induce membrane deformation, which require precise control and careful characterization of the coupled external forces. It is challenging to establish the stress-strain relationship, which is typically required for quantitative fatigue analysis. An alternative approach for probing RBC deformability based on electrokinetic forces in microfluidics has shown flexibility and ease in implementation and force characterization [37–39]. This approach can be further tuned to generate small deformations of cells based on the dielectric properties of cells and surrounding medium [40–42]. However, a quantitative study of dynamic fatigue behavior of RBCs has not yet been achieved using this approach.

In this study, we develop a new technique for dynamic fatigue measurement of single cells using programmable electrokinetic force field in microfluidics. We demonstrate the capability of this technique using normal human RBCs and further validate with adenosine triphosphate (ATP)-depleted RBCs that are known to be stiffer than normal cells [27,43,44]. The selection of RBCs over other cell types was based on the marked similarity in the cyclic mechanical stresses that circulating RBCs encounter *in vivo* and the weakening of structural materials subjected to cyclic loads in service. Viscoelastic behaviors of individually tracked RBCs in response to cyclic stretching and sudden release of the load are quantified by cellular transient deformation and characteristic response time using a Kelvin-Voigt solid model [45]. Biomechanical parameters, including membrane shear elastic modulus and shear viscosity are calculated and compared to the standards in the field for validation. This is motivated by the availability of the results from prior independent experiments using optical tweezers and micropipette aspiration as well as a similarity in the form of membrane deformation.

2. Materials and methods

2.1. Sample preparation

Blood specimens were obtained from 4 healthy donors (3 male and 1 female, aged from 26 to 54 years) with 3 specimens collected in anticoagulant EDTA tubes from local blood bank (Continental Services Group, Fort Lauderdale, USA) and 1 specimen from finger pricking. Isotonic working buffer containing 8.5% (w/v) sucrose and 0.3% (w/v) dextrose was prepared following a published protocol [46]. Its electrical conductivity was adjusted to 0.018 S/m using phosphate-buffered saline (PBS, Lonza Walkersville, Inc., Walkersville, MD). All blood specimens were measured within 3 days of blood withdrawal. Upon measurements, blood specimens were washed twice with PBS at 2000 rpm for 2 min at room temperature. RBC pellet was collected and diluted to 10^6 cells/ml in the working buffer. RBC suspension was injected into the microfluidic device and allowed to sediment for mechanical measurement. Considering the finite depth of the microfluidic device (described below), when cells sediment, cell density (cells over area) increased, allowing us to measure multiple single cells simultaneously while avoiding cell-cell interactions that may interfere with the electric field. ATP-depleted RBCs were prepared with blood specimen from a finger prick and followed with metabolic depletion [47]. Briefly, washed RBC pellet was suspended in glucose-free PBS and incubated at 37 °C for 24 h. Cell suspension was gently mixed for two times during incubation. Following incubation, RBCs were washed twice in PBS and re-suspended into the DEP working buffer for measurement. Considering the significantly lower dextrose concentration (0.3% w/v, 0.016 mM) in DEP working buffer than normal blood (4–5.9 mM) [48], regeneration of cellular ATP in incubated RBCs during measurement was expected to be small.

2.2. Microfluidic device

The microfluidic device consisted of a 50 μm deep, 500 μm wide and 10 mm long polydimethylsiloxane (PDMS) micro-channel and a 0.7 mm thick glass chip coated with an interdigitated thin-film electrode array (IEA) (Fig. 1a). The two parts were permanently

bonded using air plasma. IEA was fabricated by depositing a Ti (10 nm)/Au (100 nm) film on the glass substrate and patterned using standard microfabrication techniques, following established protocols [39]. The IEA structure consisted of 20 μm gap and 20 μm band width (Fig. 1a inset). Large deformation of RBCs was achieved by applying a high frequency sinusoid waveform through the IEA using a function generator (SIGLENT SDG830, SIGLENT, China). RBC deformation was visualized via a high-resolution GigE Camera (The Imaging Source, Charlotte, NC) mounted on a Nikon Eclipse TE2000-S inverted microscope. A 414 ± 46 nm band pass filter was inserted in the optical path for improved visualization, as this wavelength is near the peak of the hemoglobin absorption spectra [49]. This allows us to detect whether membrane rupture occurs for hemoglobin release, or cell lysis along with cell deformation. Before the mechanical testing, the microfluidic channel was coated with the working buffer containing 5% bovine serum albumin (BSA, Lot 20150520AS, Rocky Mountain Biologicals, Inc., Missoula, MT) for 30 min. Excess BSA in the channel was removed with the working buffer. This process is important to prevent cell adhesion to the bottom surface of the channel during the repeated loading.

2.3. Electrically coupled biomechanics

Electrically coupled biomechanics method using electrokinetic forces offers a new opportunity for high throughput characterization of single cells [39]. The key technique is dielectrophoresis (DEP), due to the interfacial Maxwell–Wagner polarization across cellular membranes [50]. In a conventional setup, DEP refers to migration of uncharged particles due to the induced dipole moment in a non-uniform electric field, and thus has been primarily used to separate different cell populations in combination with other microflow strategies [51,52]. When the particle is more polarizable than the surrounding medium, it moves toward the maximum electric strength gradient at the electrode edges, as indicated in the surface plot of $\log10(\nabla \boldsymbol{E}^2_{rms})$ (Fig. 2a), simulated by COMSOL Multiphysics (COMSOL, Inc., Burlington, MA). In the case of deformable biological cells, such as RBCs, they can be firmly trapped at the electrode edges and exhibit morphological deformation due to the repelling force at one of the induced dipole away from the electrode edges (Fig. 2a inset).

To quantify the DEP stretching force exerted on the cell membranes, a stretched RBC is assumed to be an ellipsoid. The time-averaged DEP force can then be estimated by [53]

$$\langle F_{DEP} \rangle = \pi abc \cdot \varepsilon_m \cdot Re(f_{CM}) \cdot \nabla E^2_{rms} \tag{1}$$

where a and b are the radii along x and y axes of the RBC, c is the thickness of the RBC, ε_m is the permittivity of the surrounding medium, and E_{rms} is the root-mean-square value of the electric field strength. $\mathrm{Re}(f_{CM})$ is the real part of the Clausius-Mossotti factor (f_{CM}). As a RBC consists of membrane and cytoplasm, its effective permittivity can be estimated with a single-shell structure, following a concentric multi-shell model [54,55],

$$f_{CM} = \frac{1}{3} \frac{(\varepsilon^*_{mem} - \varepsilon^*_m)[\varepsilon^*_{mem} + A_1(\varepsilon^*_{cyto} - \varepsilon^*_{mem})] + \rho(\varepsilon^*_{cyto} - \varepsilon^*_{mem})[\varepsilon^*_{mem} - A_1(\varepsilon^*_{mem} - \varepsilon^*_m)]}{(\varepsilon^*_m + A_1(\varepsilon^*_{mem} - \varepsilon^*_m))[\varepsilon^*_{mem} + A_1(\varepsilon^*_{cyto} - \varepsilon^*_{mem})] + \rho A_2(1 - A_2)(\varepsilon^*_{cyto} - \varepsilon^*_{mem})(\varepsilon^*_{mem} - \varepsilon^*_m)} \tag{2}$$

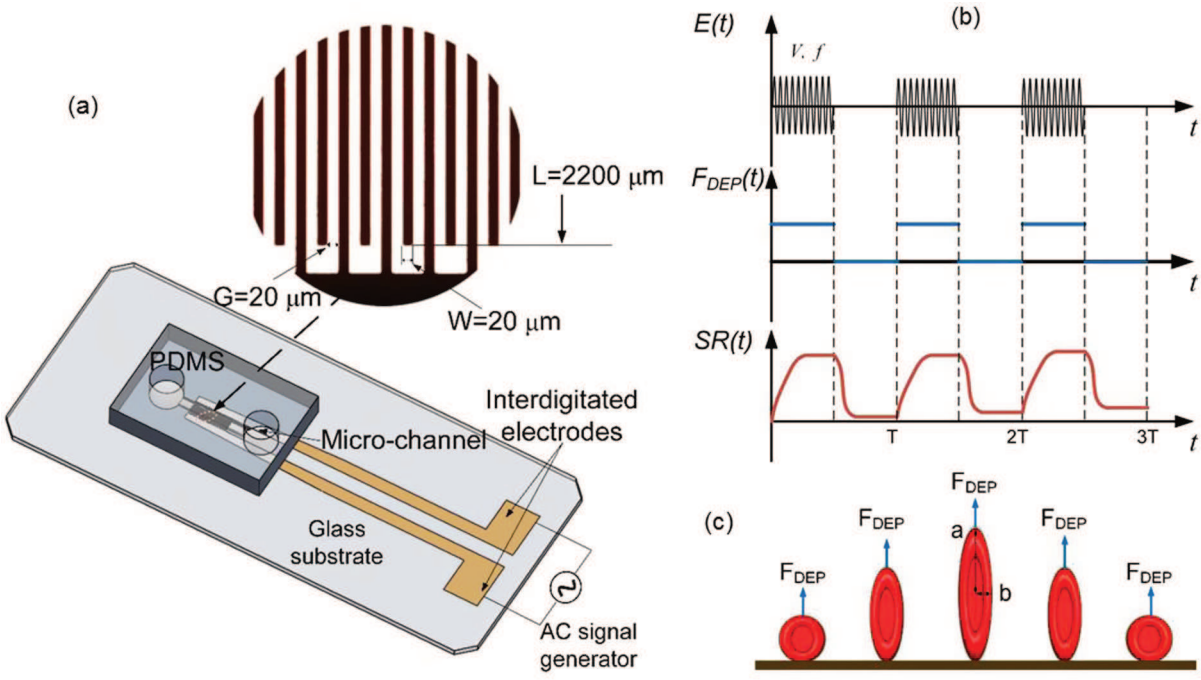

Fig. 1. Dynamic fatigue analysis of erythrocytes using DEP force field. (a) Schematic of the DEP microfluidic device with inset of interdigitated microelectrodes. (b) Amplitude modulated DEP force for cyclic tensile stretching and extensile recovery of RBCs: top panel represents the mechanical loading strategy, E(t) – ON/OFF Keying modulated high frequency electrical excitation; middle panel represents the cyclic DEP loading-release in a near square waveform, and bottom panel represents corresponding cellular stretching-recovery responses. (c) Schematic of RBC tensile stretching and extensional recovery in each loading period (from left to right).

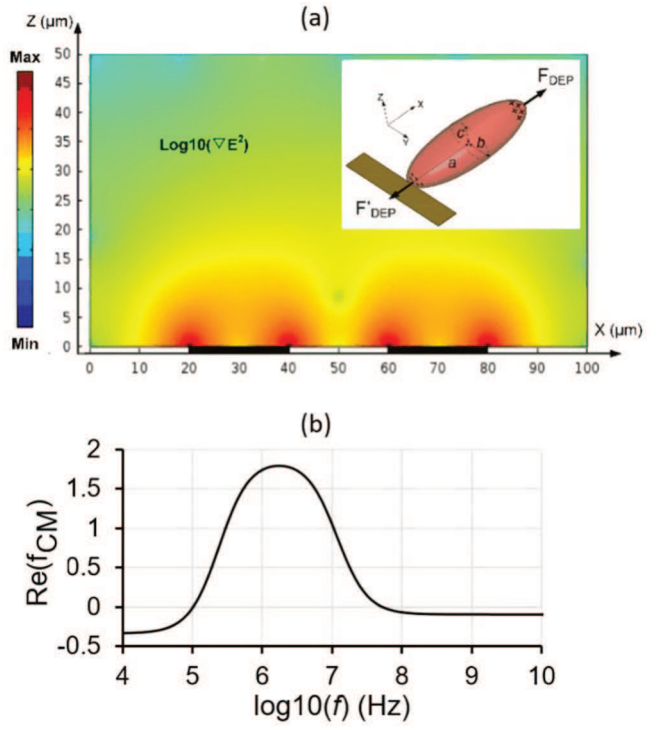

Fig. 2. Calculation of the DEP force field. (a) Surface plot of the electric field with inset of a deformed RBC due to positive DEP forces. (b) Relative DEP response of RBCs as a function of electrical frequency in the working medium.

where the subscripts *cyto*, *mem* and *m* stand for cytoplasm, membrane and medium, respectively. $\varepsilon^* = \varepsilon - i\sigma/\omega$ with ω being the angular frequency, εandσ as the dielectric permittivity and conductivity, respectively. $\rho = (a-t)(b-t)^2/(ab^2)$. Particularly, $\varepsilon_{mem} = 4.44$, $\varepsilon_{cyto} = 59$, $\sigma_{mem} = 10^{-6}$ S/m, $\sigma_{cyto} = 0.31$ S/m, adopted from other publication [56]. $A_{i=1,2}$ is the depolarization factor, defined by

$$A_i = \frac{1-e_i^2}{2e_i^3}\left[log\left(\frac{1+e_i}{1-e_i}\right) - 2e_i\right], \quad i = 1,2 \tag{3}$$

where $e_1 = \sqrt{1-\left(\frac{b-t}{a-t}\right)^2}$, $e_2 = \sqrt{1-\left(\frac{b}{a}\right)^2}$,with t being the thickness of cell membrane, 4.5 nm. Values for a and b were measured from experimental images of individual cells, and c was assumed as a constant of 2.5 μm, as the deformation mainly takes place along x–y plane according to the experimental observations. Re(f_{CM}) for RBCs were calculated using a custom script in Matlab R2010b (MathWorks, Natick, MA, see S4 in the Supplementary material). RBCs suspended in the 0.018 S/m working medium at room temperature are expected to be stretched by positive DEP forces, represented by positive values of Re(f_{CM}) with electrical frequencies between 100 kHz and 50 MHz (Fig. 2b).

The selection of electrical field strength to activate DEP force field was based on prior studies on the threshold values of electrical field strength, 2.1 kV/cm [57] and mechanical stress, 160 dynes/cm^2 [58] to avoid induction of pores or shear damage erythrocyte membranes in a non-physiological manner. In our study, strength of electrical field was 1 kV/m. The corresponding DEP force field induced shear stress was about 48 dynes/cm^2, calculated based on the mean membrane shear stress, 22 pN/μm across the mean minor axis, 4.6 μm of stretched RBCs. In present study, RBCs were suspended in an isotonic buffer, no obvious signs of hemoglobin release, membrane loss, or characteristics of electroporation [59] of cell membranes, such as cell swelling or lysis were observed. These experimental conditions allowed us to probe the mechanical deterioration in RBC membranes primarily from the cyclic stresses rather than other factors.

2.4. Cyclic loading via amplitude modulated DEP

Amplitude Shift Keying (ASK) is a form of modulation for digital data transmission over optical fibers. Here we use this technique to modulate the DEP forces. Specifically, an ON/OFF ASK was used to modulate a high frequency sinusoid waveform of 2 V_{rms} at 1.58 MHz, selected based on our previous work [60]. The modulated waveform is a high-frequency sinusoid waveform enveloped in a low-frequency square waveform (Fig. 1b). Correspondingly, a cyclic ON/OFF DEP loading is generated, including positive DEP force-induced tensile stress for 10 s, followed by a sudden release of the load, and a load-free state for 10 s. Thus, multiple cells can be probed simultaneously for their stretching and extensional recovery responses in response to the cyclic stresses (see Video S1 in the Supplementary material), yielding the new method a relatively higher throughput comparing to the classical biomechanical techniques, such as micropipette aspiration and optical tweezers with limited throughput and typically one cell at a time. During each loading cycle, dynamic response of a same cell can be monitored (see Video S2 in the Supplementary material).

2.5. Dynamic behavior and viscoelasticity analysis

Transient deformation of a RBC was quantified by its SR = a/b (Fig. 1c), using ImageJ [61]. In response to the near step-wise DEP stretching force, RBCs can reach to a maximum SR due to an equilibrium between the stretching force and the membrane elastic force resultant in a finite time. Upon a sudden release of DEP force field, stretched RBCs recover to their resting shapes in another finite time. Cumulative effects of cyclic stresses on RBC membrane deformability can then be identified for individually tracked cells by comparing its SR profiles and characteristic times of cellular recovery across the loading cycles.

In present study, we analyzed nonlinear viscoelastic deformation of RBC membranes by two parameters, including the characteristic time during the extensional recovery and the maximum SR. The maximum SR is measured at the time when the cell reaches to its equilibrium state during the loading process. RBC membrane structure is commonly modeled as an incompressible continuum. Membrane shear elasticity, μ (expressed in units of force per unit length) can be determined from the constitutive model developed by Evans and Hochmuth [45],

$$T_s = 2\mu\gamma_s = \frac{\mu}{2}(\lambda_1^2 - \lambda_2^2) \tag{4}$$

where $T_s = (T_1 - T_2)/2$, is the membrane shear stress determined from the in-plane principal membrane stresses, T_1 and T_2, γ_s is the shear strain determined from the in-plane principal extension ratios λ_1 and λ_2. The total membrane area is assumed a constant during deformation so that $\lambda_1 * \lambda_2 = 1$. The shear stress $T_s = T_1/2$, is determined from the DEP force applied to the minor diameter, *2b*, of the deformed cell membrane,

$$T_s = \frac{\langle F_{DEP}\rangle}{4b} \tag{5}$$

During the extensional recovery process after large deformation, membrane viscosity dominates the energy dissipation and can be interpreted by a Kelvin-Voigt solid model,

$$\frac{T_s}{2\mu} = \frac{1}{4}(SR^2 - SR^{-2}) + t_c\frac{\partial \ln SR}{\partial t} \tag{6}$$

where $t_c \equiv \eta/\mu$ is the material time constant that characterizes extensional response to force changes in the membrane. The above equation describes SR in the nonlinear regimes of cell membranes experiencing large deformation. Upon sudden release of DEP force, the left-hand side of the equation that represents the membrane elastic force resultant becomes zero [62]. Integration of the equation gives the recovery characteristic time, t_c required for the RBC membrane to recover to its resting stress-free shape. For convenience, with a definition of $\Lambda \equiv (SR_0 + SR_\infty)/(SR_0 - SR_\infty)$, where SR_0 and SR_∞ represent the cellular SR at the point of DEP release and when membrane recovers to the stress-free state, the solution of the transient SR can be written as,

$$\mathrm{SR(t)} = \mathrm{SR}_\infty \frac{\Lambda + \exp(-\mathrm{t/t_c})}{\Lambda - \exp(-\mathrm{t/t_c})} \tag{7}$$

Correspondingly, the recovery characteristic time t_c can be extracted by an exponential fit of the experimental measurements of SR,

$$\exp(-t/t_c) = \frac{(SR - SR_\infty)(SR_0 + SR_\infty)}{(SR + SR_\infty)(SR_0 - SR_\infty)} \tag{8}$$

2.6. Statistical analyses

RBCs were individually tracked over time during the experiments for analysis. Statistical analyses were performed with OriginPro 9 (OriginLab, Northampton, MA). All data were expressed as mean ± SD, unless stated otherwise. A paired *t*-test between measurements of samples from the initial cycle and subsequent cycles was used to generate the *p*-values. A two-sample *t*-test of measurements between normal and ATP-depleted RBCs was used to generate the *p*-values. *P*-values of 0.05 or less were considered significant. For correlation studies, R^2 denotes the R-squared value.

3. Results

3.1. Dynamic behavior of RBCs

RBC membranes deformed rapidly at a time-dependent rate and reached to an equilibrium when subjected to the near step-wise stress from modulated high-frequency excitations; upon the sudden release of DEP force field, cell membrane recovered to its stress-free state rapidly at a time-dependent rate. Fig. 3a is a time sequence of microscopic images of a representative normal cell, undergoing DEP-induced stretching and subsequent recovery due to a sudden release of the DEP force during a series of stress cycles, N = 1, 10, 50, 100 and 180, respectively. Fig. 3b shows the corresponding quantitative measurement of SR as a function of time in these representative cycles. In each loading cycle, cell membranes deformed under axial tension along the direction of DEP force. Initially, RBCs exhibited a biconcave, disc shape. During each cycle, in response to the sudden activation of high frequency electric excitation, cell membranes deformed rapidly. After a sufficient number of load cycles, the rate of cell membrane deformation decreased. For instance, within the first 100 ms of each tensile stretching process, the cell deformation reached to its steady state maximum SR during the first cycle, N = 1 but not in the subsequent cycles, e.g. N = 50, 100 and 180. In addition, the tensile stretching process lasted for 10 s, providing sufficient time for all cells to deform to individual maximum levels. Such steady state maximum SR decreased with the loading cycles, as seen at the point of load release. When the DEP force is suddenly removed by turning off the electric excitation, the stretched cell gradually recovers to its stress-free state. Changes in the speed of cellular responses were observed after the cells were stressed for a large number of loading cycles.

During the tensile stretching and extensional recovery processes, RBC membranes exhibited a typical viscoelastic behavior, or viscoelastic creep behavior and deformed at a time-dependent rate. Both stretching and extensional recovery processes can be well fitted with a simple exponential function, $SR(t) = y_0 + A \cdot \exp(-t/t_c)$ for each individual loading cycles with R^2 values greater than 0.92 (Fig. 4). The hysteresis loops of SR-time for the first 0.6 s of the tensile stretching and extensional recovery processes showed an evolution in viscoelastic behavior of cell membranes, indicating a direct influence from the cyclic loads (Fig. 5a). Steady state maximum SR of RBCs decreased progressively with the number of cyclic loads under the control of applied electric field strength, indicating an increase in the stiffness of RBC membranes and shear modulus (see following analysis). Fitting Eq. (8) to the experimental data gives a value for the recovery characteristic time, t_c (Fig. 5b). Values of t_c for this representative cell were found to be 0.17 s for N = 1 and increased to 0.19 s, 0.21 s, 0.26 s, and 0.41 s for N = 10, 50, 100, and 180, respectively.

3.2. Viscoelasticity of cell membranes and validation

Based on the 50 individually tracked normal RBCs, we calculated the membrane shear modulus from Eqs. (4) and (5), and membrane shear viscosity from $t_c \equiv \eta/\mu$. To our knowledge, fatigue analysis has not yet been implemented in other classical systems. Therefore, for validation purpose, the new results on the viscoelastic parameters determined from the first loading-unloading cycle were compared to the standards in the field from independent experiments using classical optical tweezers and micropipette aspiration techniques.

Membrane shear modulus of normal RBCs determined from DEP stretching ranged from 1.9 μN/m to 30.3 μN/m (Fig. 6a). The median value was estimated to be 8.9 μN/m, which is consistent with the results obtained from micropipette aspiration, 2.4–11.3 μN/m [17,18] and optical tweezers measurements, 8.5 μN/m [20]. Characteristic time, t_c from the DEP experiments was about 0.16 ± 0.10 s (n = 50), which is consistent with the results by micropipette aspiration, 0.13 ± 0.05 s (n = 100) [45] and by optical tweezers, 0.19 ± 0.06 s (n = 8) [15]. The corresponding membrane shear viscosity from DEP experiments was estimated to be 0.1–4.2 (μN/m) s exclusive outliers (Fig. 6b). The median value was estimated as 1 (μN/m) s, in agreement with the results obtained by micropipette aspiration, 0.6–2.7 (μN/m) s [18] and by optical tweezers, 0.3–2.8 (μN/m) s [63]. In this manner, the validated new results from DEP experiments can provide a baseline to identify fatigue failure in erythrocyte membranes through a number of parameters with statistical significance, including SR, t_c, shear elasticity and viscosity (discussed in following section). The slight differences among these independent studies are likely attributed to variations in cellular history of *in vivo* circulation and cell density within a same sample and across different samples before blood withdrawal, as well as the resolution of microscopic imaging in different systems.

3.3. Cumulative fatigue damage in cell membranes

Cumulative fatigue damage was observed in both normal RBCs and ATP-depleted cells, evaluated using maximum SR and t_c (Fig. 7). Under the cyclic stresses from the same strength of electric field, maximum SR of normal RBCs decreased with the number of loading cycles, indicating an increased resistance to deformation. Maximum SR decreased slightly from 3.80 ± 0.71 for N = 1 to 3.75 ± 0.68 for N = 10 (Fig. 7a). It further decreased to 3.62 ± 0.77

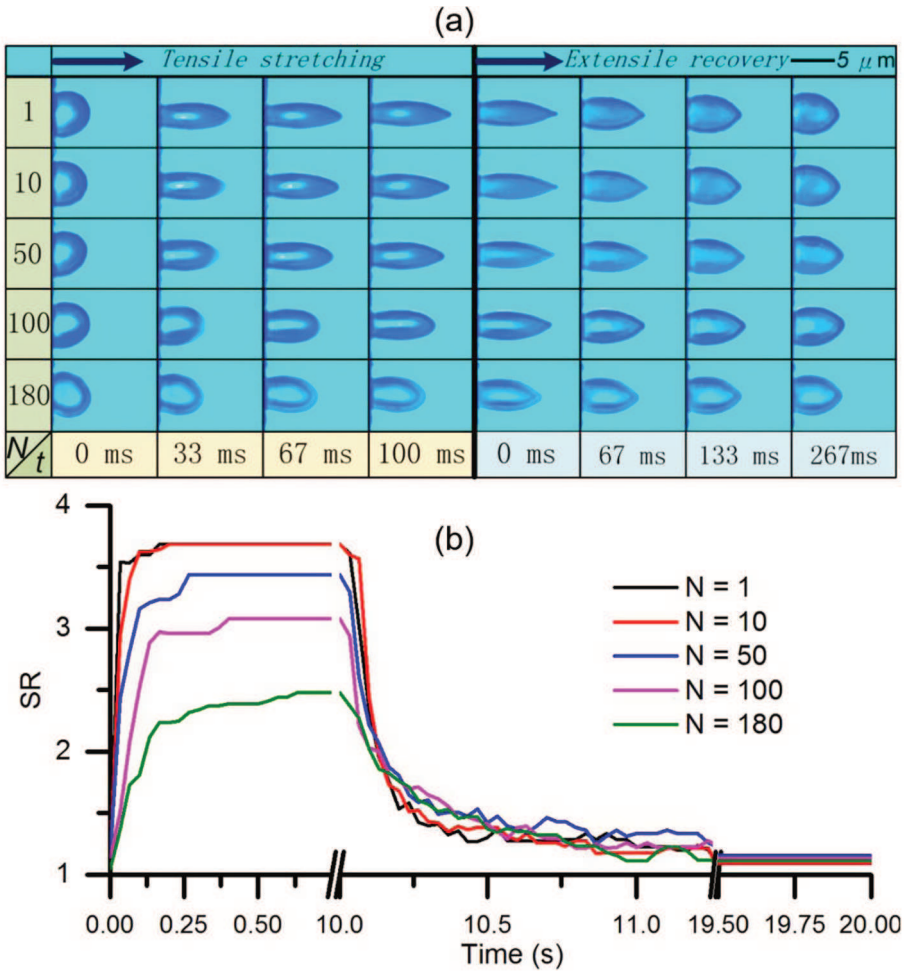

Fig. 3. Deformations of a representative RBC in response to the cyclic DEP loading-release: (a) time sequences of microscopic images of a representative cell deformation for N = 1, 10, 50, 100 and 180; (b) instantaneous SR of cell membrane as a function of time for N = 1, 10, 50, 100 and 180.

after N = 50 ($p < 0.05$) and 3.49 ± 0.82 and 2.86 ± 0.60 after 100 and 180 loading cycles, significantly different from the first cycle ($p < 0.001$), indicating the membrane stiffness increased drastically. This membrane stiffening process suggests a cyclic stress-induced damage in the structural membrane protein spectrin, which has been demonstrated to be primarily responsible for the shear elasticity of the membrane [18,64]. The recovery characteristic time, t_c increased with the number of loading cycles (Fig. 7b). Value of t_c increased from 0.16 ± 0.10 s for N = 1 and N = 10 to 0.19 ± 0.12 s, 0.24 ± 0.14 s, and 0.37 ± 0.26 s for N = 50, 100, and 180, respectively. Comparing with the first cycle, values of t_c after cyclic stresses are significantly different ($p < 0.001$ after 50 cycles). Such noticeable increase in the characteristic time indicated an increased membrane shear viscosity. Emergence of a cell with long recovery characteristic time, $t_c > 1$ s was observed after N = 180 (Fig. 7b). However, no correlations were found among the outliers for SR and t_c. This suggests that a cell with high membrane shear elasticity does not necessarily have high viscosity, and vice versa.

Variations in morphological and biomechanical measurements along with the cyclic stresses could provide an insight on cumulative deterioration in membrane mechanical integrity, in a quantitative manner. The maximum SR decreased gradually within a relatively smaller number of cyclic loads (5% decrease, $p < 0.05$, N = 50) but decreased drastically, 25% after a relatively large number of cyclic loads (N = 180). Interesting, the recovery characteristic time, t_c was found to be significantly higher after 50 loading cycles than the initial cycle (23% increase, $p < 0.001$, Fig. 7b). Correspondingly, after 50 cyclic stresses, membrane shear elastic modulus and membrane shear viscosity increased by 7% and 40%, respectively. Additionally, a direct sign of cumulative deterioration in cell membrane integrity is the emergence of irreversibly deformed cells (n = 2 out of 50) after cyclic stresses (N = 180) (see Video S3 in the Supplementary material). These findings suggest a likely sequence in membrane failure with cyclic stresses, starting with cell dehydration, membrane deformability to irreversible shape change.

ATP-depleted RBCs exhibited noticeable membrane morphological change (see Fig. S1 in the Supplementary material). ATP-depleted cells (n = 26) were tracked individually under the cyclic stresses using the same strength of electric field. Maximum SR decreased from 3.18 ± 0.60 for N = 1 to 3.17 ± 0.57, 3.21 ± 0.60, 3.00 ± 0.68 and 2.87 ± 0.94 for N = 10, 50, 100 and 180, respectively (Fig. 7c). Comparing to the normal RBCs, values of maximum SR were lower and significantly different during initial cycles ($p < 0.001$ for N = 1, 10, $p < 0.05$ for N = 50), indicating a more rigid membrane after ATP depletion, in consistency with other chemically stiffened cell membranes [65]. However, unlike normal cells, no statistically significant difference was observed between the initial and terminating cycles. The recovery characteristic time, t_c of ATP-depleted RBCs increased with the number of loading cycles, from 0.17 ± 0.10 s and 0.16 ± 0.11 s for N = 1 and 10 to 0.23 ± 0.11 s, 0.29 ± 0.17 s and 0.52 ± 0.42 s for N = 50, 100, and

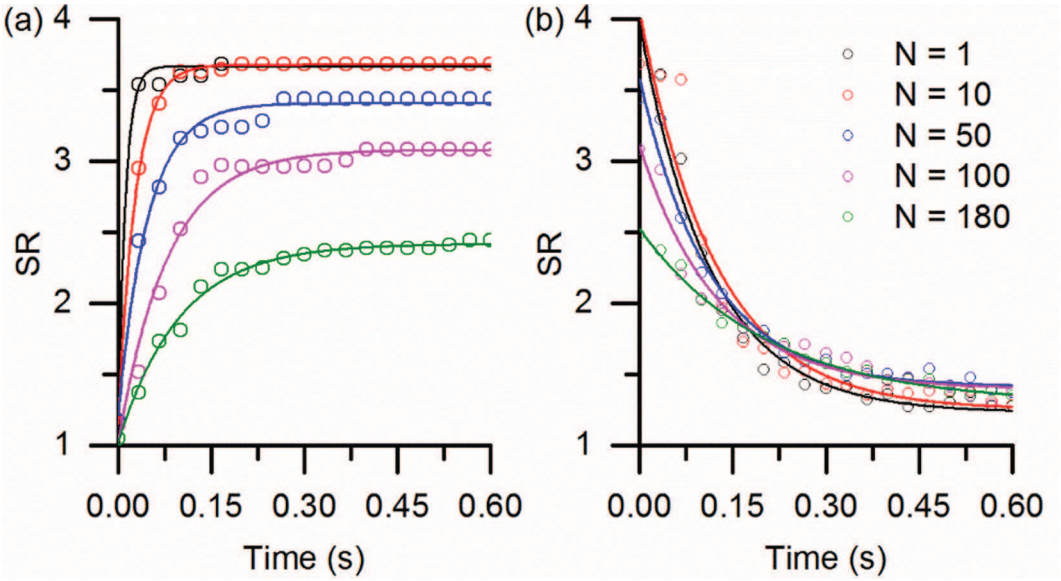

Fig. 4. Exponential fit to the cellular dynamic behavior for representative cycles N = 1, 10, 50, 100 and 180 in a representative cell: (a) creep response of cell membranes in response to stretching load; (b) extensional recovery of stretched cell membranes in response to sudden release of DEP forces. Open circles represent experimental measurement and solid curves represent exponential fit, in the form of $SR(t) = y_0 + A * \exp(-t/t_c)$ Two subplots share a same color code.

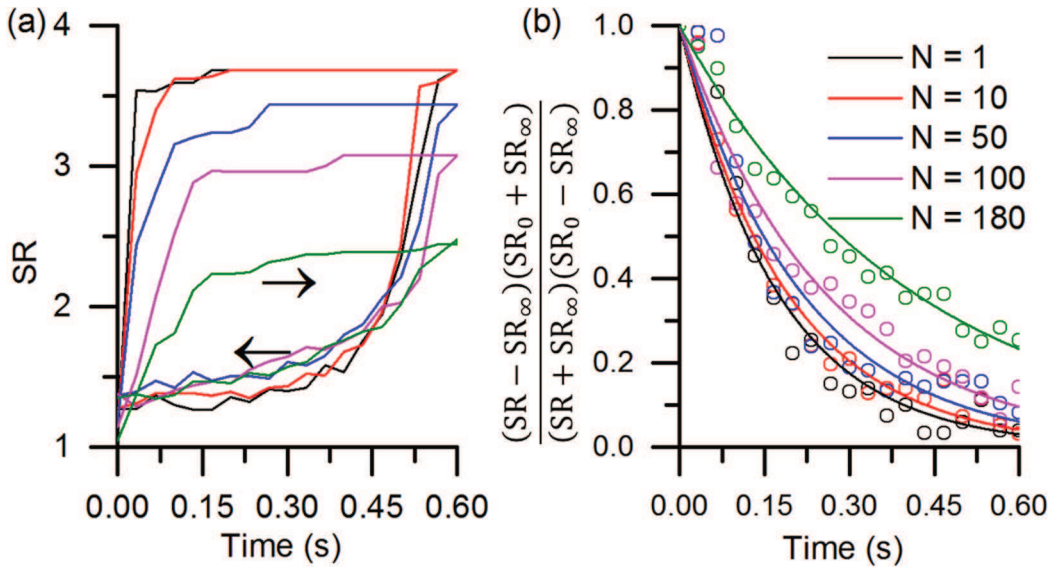

Fig. 5. Dynamic behavior of cell membrane under cyclic loads for a representative cell: (a) viscoelastic behavior, (b) extensional recovery behavior. The arrows in (a) indicate the sense of the hysteresis loops. Two subplots share a same color code.

180, respectively (Fig. 7d). Increase in the values of t_c after cyclic stresses are significant ($p < 0.001$ after 50 cycles). No statistically significant difference in t_c was found between the normal and ATP-depleted RBCs, indicating no significant change in membrane viscosity after ATP depletion.

Quantitative sensitivity of membrane viscoelastic responses to cyclic stresses in normal RBCs were displayed in Fig. 8. Correlation between the averaged maximum SR of cells (n = 15) and the number of loading cycles was strong ($R^2 = 0.92$), with the best fit linear regression line, $SR = 3.717 - 0.007N$. Correlation between the t_c (n = 21) and the number of loading cycles was strong ($R^2 = 0.93$), with the best fit Boltzmann line $t_c = 0.162 \times (1 - 1/exp((N - 111.4)/19.7))$. Value of t_c increases gradually at first, then more rapidly near N = 100, and reaches to a saturate level near N = 150. The decreased maximum SR, increased t_c along with the number of load cycles were observed widely when individual cells were tracked over time. The variations in SR and t_c along with the loading cycles across the individually tracked cells are consistent with the average of the population.

3.4. Membrane viscoelasticity during cyclic deformation

Median membrane shear modulus of normal RBCs was estimated to be 8.9 μN/m, 9.3 μN/m, and 9.6 μN/m for N = 1, 10, and 50, respectively, indicating a process of cell stiffening in response to cyclic stresses. The membrane shear modulus was estimated to be 7.9 μN/m and 5.8 μN/m for N = 100 and N = 180, respectively. Due to the significantly reduced SR after 100 cycles

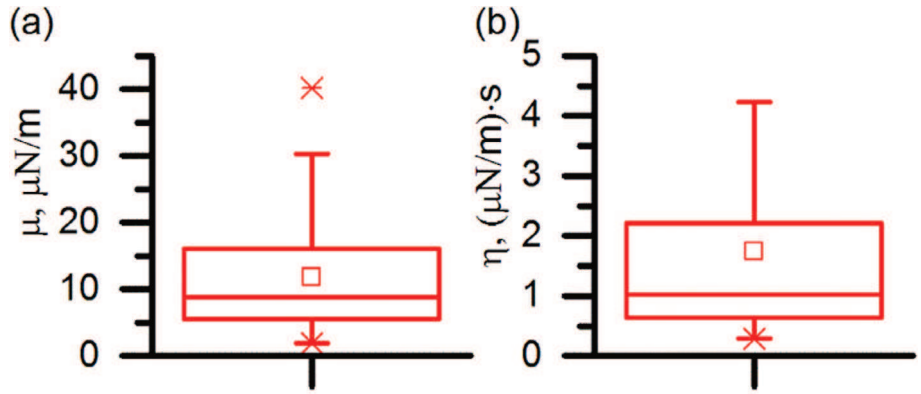

Fig. 6. Membrane shear elastic modulus (a) and membrane viscosity (b) of individually tracked normal RBCs (n = 50).

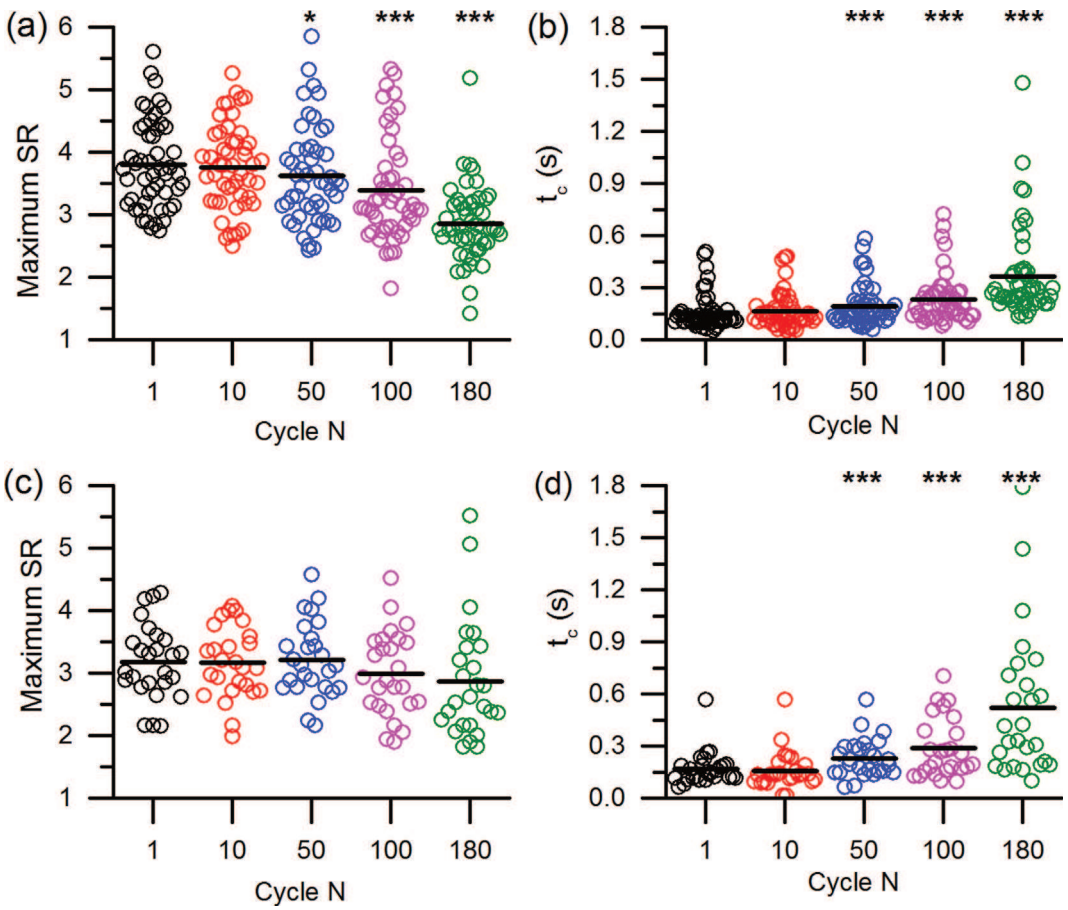

Fig. 7. Dynamic behavior of normal RBCs (n = 50) and ATP-depleted RBCs (n = 26) in response to cyclic loads. (a) Maximum SR of normal RBCs, 3.80 ± 0.71, 3.75 ± 0.68, 3.62 ± 0.77, 3.49 ± 0.82 and 2.86 ± 0.60 for N = 1, 10, 50, 100, and 180, respectively. (b) Maximum SR of ATP-depleted RBCs, 3.18 ± 0.60, 3.17 ± 0.57, 3.21 ± 0.60, 3.00 ± 0.68 and 2.87 ± 0.94 for N = 1, 10, 50, 100, and 180, respectively. (c) Recovery characteristic time t_c of normal RBCs, 0.16 ± 0.10 s, 0.16 ± 0.10 s, 0.19 ± 0.12 s, 0.24 ± 0.14 s, and 0.37 ± 0.26 s for N = 1, 10, 50, 100, and 180, respectively. (d) Recovery characteristic time *tc* of ATP-depleted RBCs, 0.17 ± 0.10 s, 0.16 ± 0.11 s, 0.23 ± 0.11 s, 0.29 ± 0.17 s and 0.52 ± 0.42 s for N = 1, 10, 50, 100, and 180, respectively. * $p < 0.05$, ** $p < 0.01$, *** $p < 0.001$.

of repeated loads, the DEP force exerted on cell membranes decreased correspondingly. The lower membrane shear modulus after 100 cycles may be attributed to the nonlinearity in membrane elasticity, which is a function of the level of the applied shear stress [63]. The corresponding membrane shear viscosity increased from 1.0 (μN/m) s for N = 1 to 1.1 (μN/m) s, 1.4 (μN/m) s, and 1.6 (μN/m) s for N = 50, 100, and 180, respectively. With the dielectric properties of ATP-depleted RBCs taken to be approximately same as normal RBCs, membrane shear modulus and viscosity of ATP-depleted RBCs were on the same order of magnitude with normal RBCs. Median values of membrane shear modulus was estimated to be 5.7 μN/m for N = 1, and reduce to 5.3 μN/m for N = 50 and 3.8 μN/m for N = 180, respectively. The membrane viscosity was 0.9 (μN/m) s for N = 1, and increased to 1.2 (μN/m) s for N = 50 and 1.7 (μN/m) s for N = 180, respectively. The measured membrane viscosity is quite similar between normal RBCs and ATP-depleted RBCs, in agreement with other studies [47,66].

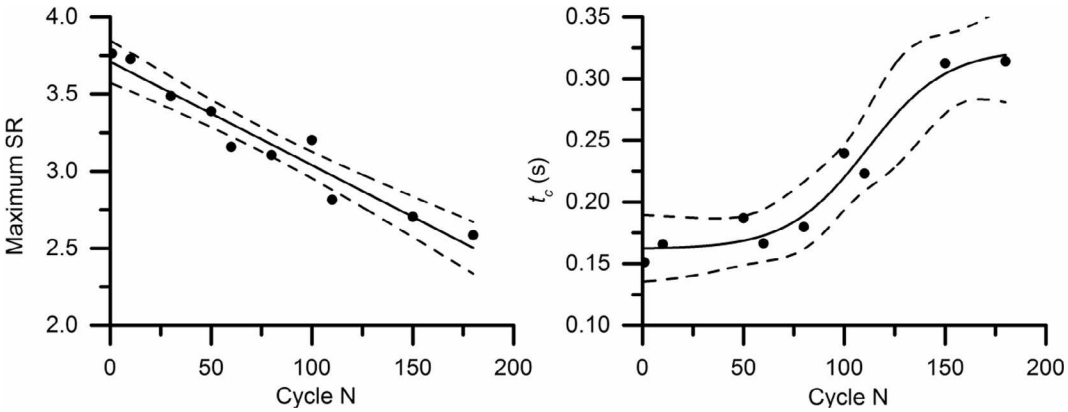

Fig. 8. Quantitative sensitivity of RBC viscoelastic responses to cyclic stresses. (a) The correlation between the maximum SR of RBCs (n = 15) and the number of loading cycles was strong (R^2 = 0.92). The solid line represents the best fit linear regression line ($SR = 3.717 - 0.007N$) and the dashed lines represent the 95% confidence interval. (b) The correlation between the t_c (n = 21) and the number of loading cycles was strong (R^2 = 0.93). The solid line represents the best fit Boltzmann line ($t_c = 0.162 \times (1 - 1/exp((N - 111.4)/19.7))$ and the dashed lines represent the 95% confidence interval.

4. Discussion

This study has demonstrated the morphological and mechanical degradation of cell membranes in normal and ATP-depleted RBCs pertaining to fatigue failure in a microfluidic platform and presents a comprehensive framework for analyzing cumulative damage induced by electrodeformation stresses in cell membranes. This method affords several advantages for cell biomechanical study. We demonstrated large deformation in cell membranes and a low cycle fatigue study. As DEP force field is generated by applying alternating current signals to the microelectrodes, it can be easily programmed to (a) impose small deformation to large deformation on single cells by adjusting the strength of the electric field, and (b) impose cyclic stress states for the study of fatigue behavior of single cells by varying the ASK frequency and amplitude. In our method, interdigitated microelectrodes were used to create asymmetric electric field so that multiple cells can be probed simultaneously. Hence, it provides a means to measure cell deformations in a relatively higher throughput comparing to the classical techniques such as optical tweezers and micropipette aspiration, which suffer from low throughput and typically measure one cell at a time.

The observed increase in membrane shear viscosity in normal and ATP-depleted RBCs is likely attributed to cell dehydration, or water loss due to a changed cation permeability from shear stress, as RBC membrane viscosity is strongly dependent on the intracellular hemoglobin concentration [67,68]. The mechanism underlying the cell dehydration may be relevant to the cyclic stresses, as isotonic buffer was used so it is less likely to induce cell dehydration from hypertonic stress. It is known that large deformation can induce changes in membrane cation permeability, as demonstrated by other prior studies [69,70]. It has also been demonstrated that dehydration in RBCs may involve stress-related activation of certain mechanosensitive ion channels, e.g. Piezo1 [71], which further activates KCa3.1 and induces efflux of K+ and consequent water loss. This is relevant to the increased cation permeability observed in RBCs deformed by patch clamping [69] and shear flow [70]. It is also possible that membrane loss may occur and lead to subtle changes in cell size, which, however, was not significant enough to be detected based on the current imaging resolution in bright field microscope. These factors may explain the markedly increased membrane shear viscosity observed after cyclic tensile stretching (40% for N = 50 and 60% for N = 180).

A consistent rise in membrane elastic modulus (from 8.9 μN/m to 9.6 μN/m) was observed in normal RBCs from N = 1 to N = 50, indicating a membrane stiffening process due to fatigue loading. This mechanical degradation is mainly attributed to the cyclic stresses rather than the influence from nonlinearity in membrane shear elasticity, as the average values of shear stress exerted on cell membranes during these cycles were quite close, from 22.0 μN/m to 21.2 μN/m. Furthermore, critical conditions can be identified to induce measurable damage in membrane integrity, depending on the specific experimental conditions. As indicated by the shear flow experiment [70], membrane deformation per se does not increase permeability unless it is beyond a critical condition, e.g. the ellipticity value of 0.75, an equivalent SR value of 7. As a comparison, in the case of cyclic stresses from DEP field and induced SR level of 3–4, a threshold number of loading cycles is N = 100 to cause a significant change in membrane elasticity and N = 50 to cause a significant change in membrane viscosity.

Values of maximum SR in ATP-depleted RBCs were significantly lower than that of normal RBCs under the cyclic stresses under the control of electric field strength. The determined membrane shear modulus in ATP-depleted RBCs were, however, lower than normal RBCs, which is different from another report showing higher shear elasticity in ATP-depleted RBC membranes [31]. The seemly conflicting observations do not necessarily indicate a stiffer or softer membrane after metabolic depletion in RBCs in our experiments. Instead, we believe such discrepancy may be attributed to several factors besides the differences in measurement techniques and samples between different studies. Remarkable nonlinear elasticity in cell membranes should be considered, e.g. from 2.5 ± 0.4 μN/m [19] to 13.3 μN/m [15] depending on the applied force level. In our study, shear stress was induced by DEP mechanism. As the DEP force is a function of cell dimensions and the gradient of electric field strength square, the shear stress exerted on cell membrane is therefore dependent on cellular extension ratio and the cell periphery at a position furthest from the electrode edge where the gradient of electric field strength square is measured. Therefore, a lower value in membrane shear modulus does not necessarily indicate a "softer" membrane without a comparable level of applied shear stress. This also explains the drop in membrane shear modulus of normal RBCs in response to cyclic stresses after 100 cycles.

The new results presented in this study can offer some useful insights into the mechanical degradation in cell membranes subjected to cyclic stretch-relaxation. It does not model other forms of mechanical stresses that RBCs in circulation could experience, e.g. tearing and bending cycles. To truly model the sophisticated

mechanical stresses that circulating RBCs encounter for a more reliable prediction of the accumulative damage in circulating RBCs, more detailed and comprehensive loading scenarios beyond uniaxial stretch-relaxation cycles need to be included. To investigate that, amplitude, loading rate, frequency, as well as the directions of the applied cyclic stresses need to be further adjusted using a combinational computation and experimental approach. This study does not include the influence of ATP depletion or other pathological states on the dielectric properties of RBCs. It is known that electrical properties of RBCs could be modified by its disease state. From prior studies, we know that malaria parasite infected erythrocytes exhibit different surface charge comparing to uninfected ones [56]. Relative permittivity, ε_r and electrical conductivity, σ of cell membrane are about $\varepsilon_r = 9.03$ and $\sigma = 7 \times 10^{-5}$ S/m for infected erythrocytes, comparing to $\varepsilon_r = 4.44$ and $\sigma < 10^{-6}$ S/m for healthy/uninfected erythrocytes. The values of cytoplasm are $\varepsilon_r = 58$ and $\sigma = 0.02$ S/m for infected cells, comparing to $\varepsilon_r = 59$ and $\sigma = 0.31$ S/m for healthy/uninfected ones. In sickle cell disease, erythrocytes have significantly higher hemoglobin concentration than healthy erythrocytes [72], which implies a higher electrical conductivity than normal cells. DEP force calibration requires inputs of cellular electrical properties. To examine quantitatively the influence of a specific human disease on the DEP stress exerted on cell membranes, a comprehensive characterization of the electrical properties of the subcellular components (Eq. (2)) is required. This will be investigated in future work by recourse to a detailed DEP analysis.

5. Concluding remarks

We have presented a new biomechanical method for characterization of dynamic fatigue behaviors of human RBCs, using ASK modulated DEP forces in a microfabricated fluid chip. We demonstrated the capability of this new technique on cell fatigue analysis using normal human RBCs as well as ATP-depleted RBCs. Dynamic behavior of normal RBCs during the initial loading cycle, quantified by morphological and biomechanical parameters, were validated by comparing to the standard values using classical biomechanical techniques such as optical tweezers and micropipette aspiration. These validated new results provided a baseline to evaluate the cumulative effects of cyclic stresses on cell membranes in both groups. These parameters showed strong correlations with the load cycles, indicating fatigue failure in cell membranes. Additionally, the rate of mechanical degradation was found to be different between normal RBCs and ATP-depleted cells, suggesting cellular physiological state may affect its resistance to fatigue loading *in vitro* and possibly indicate cellular mechanical reliability to withstand cyclic stresses *in vivo*. We envision this method can be helpful to better understand the fatigue failure of other biological cells and diseased RBCs from cyclic mechanical stresses.

Conflict-of-interest disclosure

The authors declare no competing financial interests.

Acknowledgments

This material is based upon work supported by the National Science Foundation under Grant No. 1635312 and No. 1464102. E.D. acknowledges for Florida Atlantic University faculty startup grant. Research carried out in part at the Center for Functional Nanomaterials, Brookhaven National Laboratory, which is supported by the U.S. Department of Energy, Office of Basic Energy Sciences, under Contract No. DE-SC0012704.

Appendix A. Supplementary data

Supplementary data associated with this article can be found, in the online version, at http://dx.doi.org/10.1016/j.actbio.2017.05.037.

References

[1] N. Mohandas, P.G. Gallagher, Red cell membrane: past, present, and future, Blood 112 (10) (2008) 3939–3948.
[2] K.L. Black, R.D. Jones, The discocyte-echinocyte transformation as an index of human red cell trauma, 1976.
[3] M.H. Antonelou, A.G. Kriebardis, I.S. Papassideri, Aging and death signalling in mature red cells: from basic science to transfusion practice, Blood Transfusion 8 (2010) S39–S47.
[4] A.M. Dondorp, P.A. Kager, J. Vreeken, N.J. White, Abnormal blood flow and red blood cell deformability in severe malaria, Parasitol. Today 16 (6) (2000) 228–232.
[5] A. Pellizzaro, G. Welker, D. Scott, R. Solomon, J. Cooper, A. Farone, M. Farone, R. S. Mushi, M.D.P. Aguinaga, D. Erenso, Direct laser trapping for measuring the behavior of transfused erythrocytes in a sickle cell anemia patient, Biomedical, Opt. Express 3 (9) (2012) 2190–2199.
[6] G. Cicco, A. Pirrelli, Red blood cell (RBC) deformability, RBC aggregability and tissue oxygenation in hypertension, Clin. Hemorheol. Microcirc. 21 (3, 4) (1999) 169–177.
[7] K. Tsukada, E. Sekizuka, C. Oshio, H. Minamitani, Direct measurement of erythrocyte deformability in diabetes mellitus with a transparent microchannel capillary model and high-speed video camera system, Microvasc Res. 61 (3) (2001) 231–239.
[8] H.D. Polaschegg, Red blood cell damage from extracorporeal circulation in hemodialysis, Semin. Dial. 22 (5) (2009) 524–531.
[9] K.L. Black, R.D. Jones, The discocyte-echinocyte transformation as an index of human red cell trauma, Ohio J. Sci. 75 (6) (1976) 225–230.
[10] S. Suresh, Biomechanics and biophysics of cancer cells, Acta Biomater. 3 (4) (2007) 413–438.
[11] G.A. Barabino, M.O. Platt, D.K. Kaul, Sickle cell biomechanics, Annu. Rev. Biomed. Eng. 12 (12) (2010) 345–367.
[12] D. Discher, C. Dong, J.J. Fredberg, F. Guilak, D. Ingber, P. Janmey, R.D. Kamm, G. W. Schmid-Schonbein, S. Weinbaum, Biomechanics: cell research and applications for the next decade, Ann. Biomed. Eng. 37 (5) (2009) 847–859.
[13] S. Suresh, J. Spatz, J.P. Mills, A. Micoulet, M. Dao, C.T. Lim, M. Beil, T. Seufferlein, Connections between single-cell biomechanics and human disease states: gastrointestinal cancer and malaria, Acta Biomater. 1 (1) (2005) 15–30.
[14] G.M. Artmann, K. Sung, T. Horn, D. Whittemore, G. Norwich, S. Chien, Micropipette aspiration of human erythrocytes induces echinocytes via membrane phospholipid translocation, Biophys. J. 72 (3) (1997) 1434.
[15] M. Dao, C.T. Lim, S. Suresh, Mechanics of the human red blood cell deformed by optical tweezers, J. Mech. Phys. Solids 51 (11) (2003) 2259–2280.
[16] S. Rancourt-Grenier, M.-T. Wei, J.-J. Bai, A. Chiou, P.P. Bareil, P.-L. Duval, Y. Sheng, Dynamic deformation of red blood cell in dual-trap optical tweezers, Opt. Express 18 (10) (2010) 10462–10472.
[17] S. Chien, K.L. Sung, R. Skalak, S. Usami, A. Tozeren, Theoretical and experimental studies on viscoelastic properties of erythrocyte membrane, Biophys. J. 24 (2) (1978) 463–487.
[18] R. Hochmuth, R. Waugh, Erythrocyte membrane elasticity and viscosity, Annu. Rev. Physiol. 49 (1) (1987) 209–219.
[19] S. Henon, G. Lenormand, A. Richert, F. Gallet, A new determination of the shear modulus of the human erythrocyte membrane using optical tweezers, Biophys. J. 76 (2) (1999) 1145–1151.
[20] M. Dao, J. Li, S. Suresh, Molecularly based analysis of deformation of spectrin network and human erythrocyte, Mater. Sci. Eng. C 26 (8) (2006) 1232–1244.
[21] C. Lim, E. Zhou, A. Li, S. Vedula, H. Fu, Experimental techniques for single cell and single molecule biomechanics, Mater. Sci. Eng. C 26 (8) (2006) 1278–1288.
[22] R.M. Johnson, Ektacytometry of red blood-cells, Method Enzymol. 173 (1989) 35–54.
[23] M. Puig-De-Morales-Marinkovic, K.T. Turner, J.P. Butler, J.J. Fredberg, S. Suresh, Viscoelasticity of the human red blood cell, Am. J. Physiol. 293 (2) (2007) C597–C605.
[24] R. Wang, H.F. Ding, M. Mir, K. Tangella, G. Popescu, Effective 3D viscoelasticity of red blood cells measured by diffraction phase microscopy, Biomed. Opt. Express 2 (3) (2011) 485–490.
[25] M. Musielak, Red blood cell-deformability measurement: review of techniques, Clin. Hemorheol. Microcirc. 42 (1) (2009) 47–64.
[26] Y. Kim, K. Kim, Y. Park, Measurement techniques for red blood cell deformability: recent, Advances (2012).
[27] R.I. Weed, P.L. LaCelle, E.W. Merrill, Metabolic dependence of red cell deformability, J. Clin. Invest. 48 (5) (1969) 795.
[28] R.I. Weed, P.L. Lacelle, E.W. Merrill, Metabolic dependence of red cell deformability, J. Clin. Invest. 48 (5) (1969) 795.
[29] N.S. Gov, S.A. Safran, Red blood cell membrane fluctuations and shape controlled by ATP-induced cytoskeletal defects (vol 88, pg 1859, 2005), Biophys. J. 89 (1) (2005).
[30] E. Ben-Isaac, Y. Park, G. Popescu, F.L.H. Brown, N.S. Gov, Y. Shokef, Effective temperature of red-blood-cell membrane fluctuations, Phys. Rev. Lett. 106 (23) (2011).

[31] H.J. Meiselman, E.A. Evans, R.M. Hochmuth, Membrane mechanical-properties of atp-depleted human erythrocytes, Blood 52 (3) (1978) 499–504.
[32] S. Tuvia, S. Levin, A. Bitler, R. Korenstein, Mechanical fluctuations of the membrane-skeleton are dependent on F-actin ATPase in human erythrocytes, J. Cell Biol. 141 (7) (1998) 1551–1561.
[33] T. Betz, M. Lenz, J.F. Joanny, C. Sykes, ATP-dependent mechanics of red blood cells, Proc. Natl. Acad. Sci. U.S.A. 106 (36) (2009) 15320–15325.
[34] Y.K. Park, C.A. Best, T. Auth, N.S. Gov, S.A. Safran, G. Popescu, S. Suresh, M.S. Feld, Metabolic remodeling of the human red blood cell membrane, Proc. Natl. Acad. Sci. U.S.A. 107 (4) (2010) 1289–1294.
[35] S. Sakuma, K. Kuroda, C.H.D. Tsai, W. Fukui, F. Arai, M. Kaneko, Red blood cell fatigue evaluation based on the close-encountering point between extensibility and recoverability, Lab. Chip 14 (6) (2014) 1135–1141.
[36] S. Hashimoto, Detect of sublethal damage with cyclic deformation of erythrocyte in shear flow, J. Syst. Cybern. Inf. 12 (3) (2014) 41–46.
[37] H. Engelhardt, E. Sackmann, On the measurement of shear elastic moduli and viscosities of erythrocyte plasma membranes by transient deformation in high frequency electric fields, Biophys. J. 54 (3) (1988) 495–508.
[38] H. Engelhardt, H. Gaub, E. Sackmann, Viscoelastic properties of erythrocyte membranes in high-frequency electric fields, Nature 307 (5949) (1984) 378–380.
[39] E. Du, M. Dao, S. Suresh, Quantitative biomechanics of healthy and diseased human red blood cells using dielectrophoresis in a microfluidic system, Extreme Mech. Lett. 1 (2014) 35–41.
[40] I. Guido, M.S. Jaeger, C. Duschl, Dielectrophoretic stretching of cells allows for characterization of their mechanical properties, Eur. Biophys. J. Biophys. 40 (3) (2011) 281–288.
[41] J. Chen, M. Abdelgawad, L.M. Yu, N. Shakiba, W.Y. Chien, Z. Lu, W.R. Geddie, M. A.S. Jewett, Y. Sun, Electrodeformation for single cell mechanical characterization, J. Micromech. Microeng. 21 (5) (2011).
[42] L.A. MacQueen, M.D. Buschmann, M.R. Wertheimer, Mechanical properties of mammalian cells in suspension measured by electro-deformation, J. Micromech. Microeng. 20 (6) (2010).
[43] Y. Park, C.A. Best, T. Auth, N.S. Gov, S.A. Safran, G. Popescu, S. Suresh, M.S. Feld, Metabolic remodeling of the human red blood cell membrane, Proc. Natl. Acad. Sci. 107 (4) (2010) 1289–1294.
[44] T. Betz, M. Lenz, J.-F. Joanny, C. Sykes, ATP-dependent mechanics of red blood cells, Proc. Natl. Acad. Sci. 106 (36) (2009) 15320–15325.
[45] R.M. Hochmuth, P.R. Worthy, E.A. Evans, Red cell extensional recovery and the determination of membrane viscosity, Biophys. J. 26 (1) (1979) 101–114.
[46] K. Khoshmanesh, S. Nahavandi, S. Baratchi, A. Mitchell, K. Kalantar-zadeh, Dielectrophoretic platforms for bio-microfluidic systems, Biosens. Bioelectron. 26 (5) (2011) 1800–1814.
[47] H.J. Meiselman, E.A. Evans, R.M. Hochmuth, Membrane mechanical properties of ATP-depleted human erythrocytes, Blood 52 (3) (1978) 499–504.
[48] J. Viskupicova, D. Blaskovic, S. Galiniak, M. Soszyński, G. Bartosz, L. Horakova, I. Sadowska-Bartosz, Effect of high glucose concentrations on human erythrocytes in vitro, Redox Biol. 5 (2015) 381–387.
[49] P. Chikezie, A. Akuwudike, F. Chilaka, Absorption spectra of normal adults and patients with sickle cell anaemia haemoglobins treated with hydrogen peroxide at two pH values, Iran. J. Blood Cancer 5 (4) (2013) 129–135.
[50] N.G. Green, H. Morgan, Dielectrophoretic investigations of sub-micrometre latex spheres, J. Phys. D 30 (18) (1997) 2626–2633.
[51] Z.R. Gagnon, Cellular dielectrophoresis: applications to the characterization, manipulation, separation and patterning of cells, Electrophoresis 32 (18) (2011) 2466–2487.
[52] P.R. Gascoyne, J. Vykoukal, Particle separation by dielectrophoresis, Electrophoresis 23 (13) (2002) 1973–1983.
[53] H. Morgan, N.G. Green, AC Electrokinetics, Research Studies Press, 2003.
[54] M. Castellarnau, A. Errachid, C. Madrid, A. Juarez, J. Samitier, Dielectrophoresis as a tool to characterize and differentiate isogenic mutants of *Escherichia coli*, Biophys. J. 91 (10) (2006) 3937–3945.
[55] L. Zheng, J.P. Brody, P.J. Burke, Electronic manipulation of DNA, proteins, and nanoparticles for potential circuit assembly, Biosens. Bioelectron. 20 (3) (2004) 606–619.
[56] P. Gascoyne, C. Mahidol, M. Ruchirawat, J. Satayavivad, P. Watcharasit, F.F. Becker, Microsample preparation by dielectrophoresis: isolation of malaria, Lab. Chip 2 (2) (2002) 70–75.
[57] E.H. Serpersu, K. Kinosita, T.Y. Tsong, Reversible and irreversible modification of erythrocyte-membrane permeability by electric-field, Biochim. Biophys. Acta 812 (3) (1985) 779–785.
[58] L.B. Leverett, E.C. Lynch, C.P. Alfrey, J.D. Hellums, Red blood-cell damage by shear-stress, Biophys. J. 12 (3) (1972) 257.
[59] J. Teissie, M. Golzio, M. Rols, Mechanisms of cell membrane electropermeabilization: a minireview of our present (lack of?) knowledge, Biochim. Biophys. Acta 1724 (3) (2005) 270–280.
[60] Y. Qiang, J. Liu, M. Mian, E. Du, Experimental Electromechanics of Red Blood Cells Using Dielectrophoresis-Based Microfluidics, Mechanics of Biological Systems and Materials, vol. 6, Springer, 2017, pp. 129–134.
[61] W. Rasband, ImageJ, US National Institutes of Health, Bethesda, MD, 1997.
[62] E.A. Evans, R. Waugh, L. Melnik, Elastic area compressibility modulus of red cell membrane, Biophys. J. 16 (6) (1976) 585–595.
[63] J.P. Mills, L. Qie, M. Dao, C.T. Lim, S. Suresh, Nonlinear elastic and viscoelastic deformation of the human red blood cell with optical tweezers, Mech. Chem. Biosyst. 1 (3) (2004) 169–180.
[64] R.E. Waugh, P. Agre, Reductions of erythrocyte membrane viscoelastic coefficients reflect spectrin deficiencies in hereditary spherocytosis, J. Clin. Invest. 81 (1) (1988) 133.
[65] T. Fischer, C. Haest, M. Stöhr, D. Kamp, B. Deuticke, Selective alteration of erythrocyte deformability by SH-reagents. Evidence for an involvement of spectrin in membrane shear elasticity, Biochim. Biophys. Acta 510 (2) (1978) 270–282.
[66] M.R. Clark, N. Mohandas, C. Feo, M.S. Jacobs, S.B. Shohet, Separate mechanisms of deformability loss in ATP-depleted and Ca-loaded erythrocytes, J. Clin. Invest. 67 (2) (1981) 531.
[67] G. Chetrite, R. Cassoly, Affinity of hemoglobin for the cytoplasmic fragment of human erythrocyte membrane band 3. Equilibrium measurements at physiological pH using matrix-bound proteins: the effects of ionic strength, deoxygenation and of 2,3-diphosphoglycerate, J. Mol. Biol. 185 (3) (1985) 639–644.
[68] J. Eisinger, J. Flores, J.M. Salhany, Association of cytosol hemoglobin with the membrane in intact erythrocytes, Proc. Natl. Acad. Sci. U.S.A. 79 (2) (1982) 408–412.
[69] B. Sakmann, E. Neher, Patch clamp techniques for studying ionic channels in excitable membranes, Annu. Rev. Physiol. 46 (1) (1984) 455–472.
[70] R.M. Johnson, Membrane stress increases cation permeability in red cells, Biophys. J. 67 (5) (1994) 1876.
[71] F. Sachs, Stretch-activated ion channels: what are they?, Physiology 25 (1) (2010) 50–56
[72] G.P. Rodgers, A.N. Schechter, C.T. Noguchi, Cell heterogeneity in sickle cell disease: quantitation of the erythrocyte density profile, J. Lab. Clin. Med. 106 (1) (1985) 30–37.